Letter

Generic rules for achieving room-temperature superconductivity in ternary hydrides with clathrate structures

Liangliang Liu,[1,2,*] Feng Peng,[3,*] Peng Song,[1,4] Xiaohan Liu,[1,2] Liying Zhang,[1,2] Xiaowei Huang,[1] Chunyao Niu,[5] Chengyan Liu,[2] Weifeng Zhang,[2] Yu Jia,[1,2,5,†] and Zhenyu Zhang[6,‡]

[1]*Key Laboratory for Special Functional Materials of Ministry of Education, School of Materials Science and Engineering, Henan University, Kaifeng 475004, China*

[2]*Joint Center for Theoretical Physics, Henan University, Kaifeng 475004, China*

[3]*College of Physics and Electronic Information, Luoyang Normal University, Luoyang 471022, China*

[4]*The Grainger College of Engineering, University of Illinois at Urbana-Champaign, Lincoln Hall, 702 S. Wright St., Urbana, Illinois 61801, USA*

[5]*International Laboratory for Quantum Functional Materials of Henan, Zhengzhou University, Zhengzhou 450001, China*

[6]*International Center for Quantum Design of Functional Materials (ICQD), Hefei National Laboratory for Physical Sciences at Microscale (HFNL), University of Science and Technology of China, Hefei, Anhui 230026, China*

(Received 23 June 2022; revised 4 January 2023; accepted 9 January 2023; published 17 January 2023)

The discovery of superconductors with higher superconducting transition temperatures (T_c's) at ambient physical conditions is a perpetual drive in fundamental studies and for practical applications. Here we conceptualize two generic rules for achieving this goal surrounding metal hydride superconductors. Rule 1: the metal skeletons should be composed of elements with an effective valency of 3 for efficient electron donation to hydrogen. Rule 2: the fractional occupancy of the metal ions should be ∼0.4 for maximal chemical squeezing on hydrogen. Guided by these rules, and based on first-principles approaches, we predict a collection of new hydride superconductors, including the representative examples of $CaHfH_{12}$, with T_c of ∼360 K at 300 GPa, and $CaZrH_{12}$, with T_c of ∼290 K at 200 GPa. These findings are expected to be instrumental in predictive discoveries of new high-T_c hydride superconductors at lower pressures.

DOI: 10.1103/PhysRevB.107.L020504

The realization of room-temperature superconductivity is one of the long-sought goals in condensed matter physics and material science [1,2]. For superconductivity within the framework of Bardeen-Cooper-Schrieffer theory, metallic hydrogen was predicted to be a good candidate to achieve room-temperature superconductivity [3–6]. Yet hydrogen metallization demands exceptionally high pressure, and is still uncertain at the pressure limit of 400 GPa experimentally accessible today [6–10]. Alternatively, H-rich materials, i.e., hydrides, were proposed to provide an alternative route to realizing high transition temperature (high-T_c) superconductivity, because hydrogen metallization can be accomplished under relatively lower physical pressure due to chemical compression on the hydrogen by the constituent heterogeneous atoms of the compounds [11]. Recently, a great deal of effort has been devoted to predictive discoveries of high-T_c superconductors among various hydride materials [12–21]. Compelling examples include H_3S [22], LaH_{10} [23,24], YH_9 [25], and so on. These advances convincingly demonstrate the potential of hydride compounds towards eventual definitive materialization of the much-coveted room-temperature superconductivity.

In existing explorations of clathrate hydrides such as CaH_6, YH_9, and LaH_{10} [12,15,17,26], the lattices of the metal atoms provide the supporting skeletons for the H_2 molecules to be as closely packed as possible. Here, the metal skeletons and hydrogen molecular cages are in essence mutually intercalated, with the hydrogen molecules preserving their covalent bonds, but much weakened [1,12,15]. To date, a large number of such clathrate hydrides have been identified, and their T_c's can reach as high as 200 K above the pressure of 150 GPa [15,24–27]. The predicted pressures at which these hydride superconductors become stable are much lower than the critical pressure required to metallize pure hydrogen, but are still difficultly high for experimental synthesis and measurement, and even more so for potential technological applications.

In striving for higher T_c's at lower pressures, here we propose two generic guiding rules surrounding clathrate hydride superconductors, with each rule rooted in distinct physical intuitions. Rule 1 (optimal valency rule): The skeleton materials should be composed of metal elements with an effective optimal valency (EMV) of 3, so as to serve as efficient electron donors. Rule 2 (optimal occupancy rule): With efficient charge transfer ensured by Rule 1, the fractional metal occupancy (FMO) should be ∼0.4, to further impose the highest possible chemical squeezing on the hydrogen molecules, thereby lowering the demand on physical pressure needed to stabilize the materials.

*These authors contributed equally to this work.
†Corresponding author: jiayu@zzu.edu.cn
‡Corresponding author: zhangzy@ustc.edu.cn

 ©2023 American Physical Society

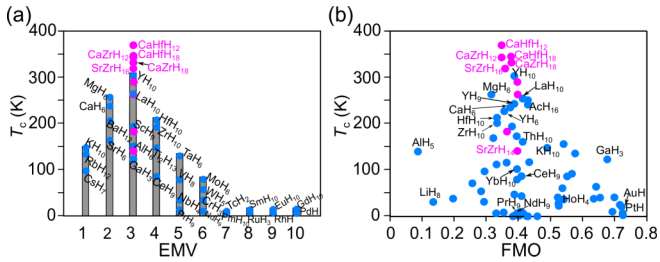

FIG. 1. The superconducting transition temperature as a function of (a) EMV and (b) FMO, respectively, labeling the effective valency and fractional volume of the metal elements in hydride superconductors. The existing systems reported in the literature are shown in blue, while the newly predicted systems in pink (see the data in Table S1 of the SM [28]).

To help rationalize Rule 1, we show in Fig. 1(a) the predicted T_c's of the hydrides as a function of the effective metal valency, or EMV, with the data in blue collected from existing literature [see Table S1 of the Supplemental Material (SM) [28]], and those newly predicted later in the present work shown in pink. We observe that, each metal atom in fcc LaH_{10} and YH_{10} has three valence electrons, and both systems exhibit the highest T_c. As the EMV increases or decreases from 3, the T_c is distinctly lowered. Intuitively, the valence electrons of the metal skeletons play the pivotal role that, upon transferring, those electrons are pumped into the antibonding σ^* orbitals of the H_2 molecules, thereby weakening the intramolecular H-H bonds due to Pauli exclusion, and potentially driving the intercalated hydrogen network into the metallic state [15]. To ensure the most effective charge transfer, the metal elements should possess the most metallic ionicity of valency, namely, 3, as an element with lower valency would be unable to provide the maximal number of transferred electrons desired, while that with much higher valency would be less willing to readily donate their valence electrons to the hydrogen molecules (due to, e.g., the Hund rule for elements containing 5*d* electrons).

To help rationalize Rule 2, we first note that the quantitative estimate on the optimal FMO is obtained by considering the commonly adopted crystalline structures of fcc, hcp, and bcc for the metal hydrides. We can again take the fcc LaH_{10} in Fig. 2(a) as an example to vividly display the chemical pressure provided by the metal skeleton. The H_2 molecules fill the interstitial space of the fcc La, elongated upon accepting electron donations from the La atoms, and squeezed by the latter as well. Therefore, the more closely packed the metal atoms, the higher the chemical pressure on the hydrogen. Meanwhile, sufficient space should still be preserved within the skeleton for the hydrogen molecules to connect and metallize. Here we focus on the well-known closely packed fcc, hcp, and bcc structures of the metal skeletons with effective metal valency of ~3. With the radii touching along the planner or bulk diagonal direction, the upper limit of the FMO is known to be ~0.74 (fcc), ~0.74 (hcp), and ~0.68 (bcc), respectively. When the intercalated H network is further included, the optimal FMO becomes $\sim 0.74/(1+r)^3$ for fcc and hcp and $\sim 0.68/(1+r)^3$ for bcc, where $r = r_H/r_M$ is the ratio of the ionic radii of H and metal atoms (see the detailed computational method in the SM [28]). Apparently, we should select metal atoms with the largest r_M's in order to maximize the chemical pressure. Figure 1(b) shows the T_c of the metal hydrides as a function of FMO, with the existing data again in blue, indicating that the clathrate hydrides with high T_c's all have a very similar FMO value of ~0.4.

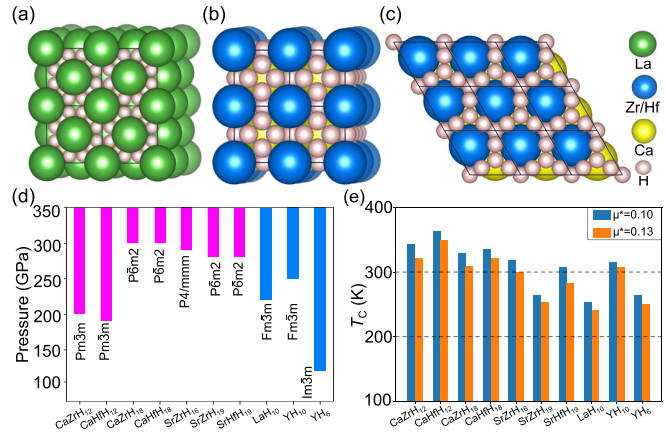

FIG. 2. Intercalated cage structures of (a) $Fm\bar{3}m$ LaH_{10}, (b) $Pm\bar{3}m$ $CaZrH_{12}$/$CaHfH_{12}$, and (c) $P\bar{6}m2$ $CaZrH_{18}$/$CaHfH_{18}$, respectively, highlighting the squeezing on the hydrogen molecules by the metal skeletons. (d) Predicted pressure-composition phase diagram of the newly predicted ternary and (e) calculated T_c's of the ternary hydrides at 300 GPa, in comparison with that of YH_6, YH_{10}, and LaH_{10} from existing studies [17,67].

With the two rules presented above, we can adventure into new materials spaces and corners for predicting new high T_c hydride superconductors. In doing so, we note that even though some existing systems such as YH_{10} and LaH_{10} already obey the two generic rules and thereby possess high T_c, its value is still much lower than ~760 K predicted for pure metallic hydrogen under an ultrahigh pressure [5,6], suggesting opportunities for even more efficient charge transfer from the metal skeletons to the hydrogen molecules. It is at present still an open issue to rigorously identify the most optimal H/metal ratio for simultaneous maximal charge transfer and chemical pressure, but as a first-order "rule of thumb," for a given H/metal combination and structure, we should work around the ratio that every valence electron of the metal is to weaken one hydrogen molecule via charge transfer and antibonding occupation. As further illustrated later, the underlying rationale is inherently tied to the optimal EMV of ~3 emphasized earlier. Furthermore, as shown in Figs. 4(c)–4(f) for a given H/metal ratio, the minimal pressure needed to stabilize the structure decreases linearly with increasing FMO, an elegant point worthy of being more fully exploited in future studies of metal hydrides.

Our searching efforts naturally expand into considerations of ternary clathrate hydrides, in which the metal element of Y or La is cosubstituted by two compensatory metal elements that possess the effective isovalency of ~3 (Rule 1, and for a latest ternary example but without obeying Rule 1, see Ref. [16]). Candidate combinations include (Ca, Sr) as one element and (Zr, Hf) as the other, with different H/metal ratios. The structural search was performed by using the swarming-intelligence based CALYPSO software [68,69]. Considering the non-negligible quantum effects associated with the relatively light H atom, the contributions of the zero-point energies were

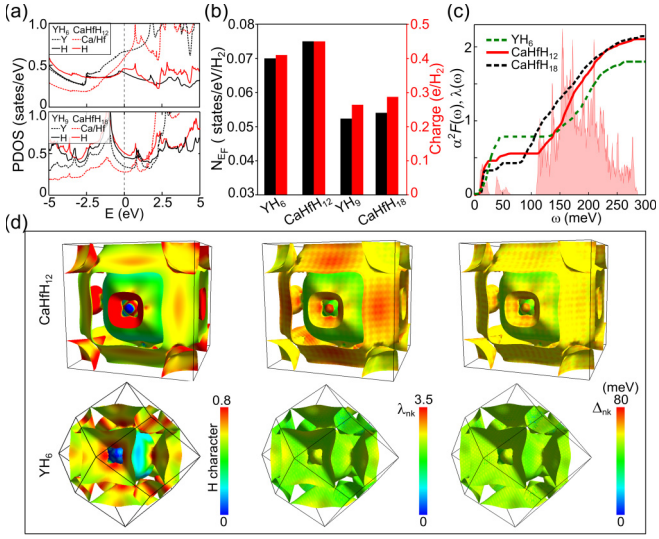

FIG. 3. (a) Atom-projected densities of states for YH_6, $CaHfH_{12}$, YH_9 and $CaHfH_{18}$ at 300 GPa. (b) H electronic states at E_F (N_{E_F}) per H_2 molecule (black) and the number of accepted electrons per H_2 molecule (red). (c) Eliashberg spectral function $\alpha^2F(\omega)$ and integrated EPC constant $\lambda(\omega)$ for $CaHfH_{12}$, in comparison with YH_6 and $CaHfH_{18}$. (d) H electronic states, k-resolved EPC strength λ_{nk}, and superconducting gap Δ_{nk} (computed at 40 K), as distributed on the Fermi surfaces of $CaHfH_{12}$ (upper column) and YH_6 (bottom column) at 300 GPa. The color scale spans the projected values.

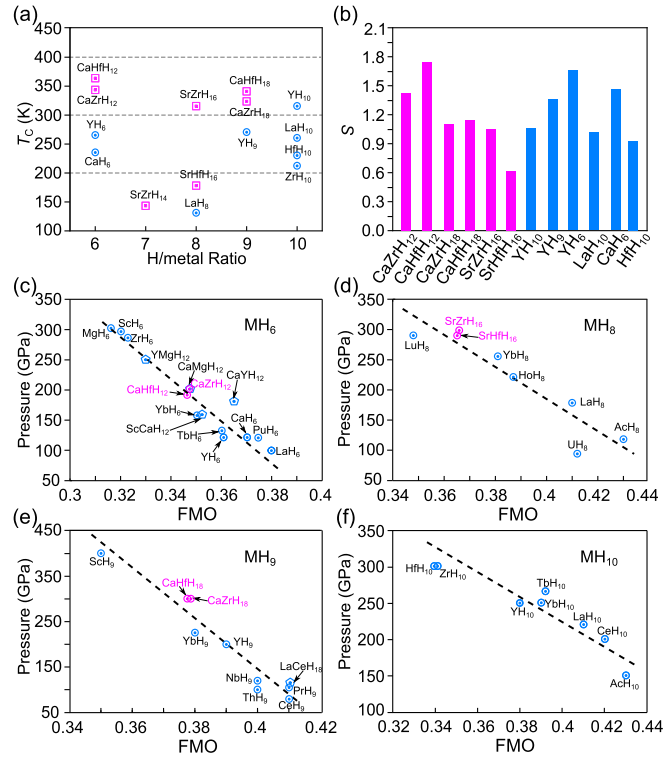

FIG. 4. (a) Dependence of T_c's of the metal hydrides on the H/metal ratio. (b) The merit function $S = \frac{T_c}{\sqrt{p^2+T_{c,MgB_2}^2}}$ [78], which seeks a compromising balance between the required pressure (P) and predicted T_c, is also used to evaluate the significance of a particular hydride superconductor. (c)–(f) The dependence of the minimum stable pressures of metal hydrides (MH_6, MH_8, MH_9, and MH_{10}) with the FMO. Here, the black dashed lines represent the linear fitting based on the scattered points. The corresponding T_c and FMO values are taken from Table S1 of the SM [28].

included in all our calculations of the formation enthalpies for the ternary hydrides. The main results of convex hull diagrams at 200, 250, and 300 GPa for $CaZrH_x$, $CaHfH_x$, $SrZrH_x$, and $SrHfH_x$ ($x = 6$–19) are shown in Figs. S1 and S2 of the SM [28], respectively. Herein, the thermodynamic stabilities of a variety of ternary hydrides were evaluated from their formation enthalpies relative to the dissociation products of mixtures of CaH_2/SrH_2 and $ZrH_3 + H_2/HfH_3 + H_2$, because the end-point compositions CaH_2, SrH_2, ZrH_3, and HfH_3 have the most negative enthalpy/atom at pressures and are chosen from the results of the previous works [12,70–72].

From our structural researching, five classes of stable structures are obtained under different pressures, including $Pm\bar{3}m$ $CaZrH_{12}/CaHfH_{12}$, $P\bar{6}m2$ $CaZrH_{18}/CaHfH_{18}$, $Cmmm$ $SrZrH_{14}$, $P4/mmm$ $SrZrH_{16}/SrHfH_{16}$, and $P\bar{6}m2$ $SrZrH_{19}/SrHfH_{19}$. $Pm\bar{3}m$ $CaZrH_{12}/CaHfH_{12}$ structures can be obtained by substituting the Y atoms in $Im\bar{3}m$ YH_6 with Ca and Hf(Zr) [13,15] [see Fig. 2(b)], and remain dynamic stability until 190–200 GPa [see Fig. 2(d)]. Here, the Ca and Zr/Hf atoms jointly form a bcc metal skeleton, and the H_2 molecules occupy its tetrahedral interstices, forming two separate H_{24} cages surrounding the Ca and Hf(Zr) atoms. The $P\bar{6}m2$ $CaZrH_{18}/CaHfH_{18}$ structures also contain two H_{29} cages surrounding the Ca and Hf(Zr) atoms [see Fig. 2(c)], while the Ca and Hf(Zr) atoms adopt a hcp skeleton, similar to the structure of $P6_3/mmc$ YH_9 [15]. In addition, our compensatory cosubstitution approach also results in new stable clathrate hydrides. Specifically, the $P4/mmm$ $SrZrH_{16}/SrHfH_{16}$ structure is bcc-like, but with the lattice constants c longer than a and b, and simultaneously contains two different types of H_2 cages [see structures in Fig. S3(a) of the SM [28]], which are similar to the H_{24} cage in the bcc YH_6 [13] and H_{32} cage in the fcc LaH_{10} [17,73], respectively. The difference is that the two H_{24} and H_{32} cages in $SrZrH_{16}/SrHfH_{16}$ possess some stretching in the c direction, with a relatively low symmetry due to the different atomic radii between Ca and Hf(Zr). The $SrZrH_{19}/SrHfH_{19}$ also adopt the $P\bar{6}m2$ space group in Fig. S3(b) of the SM [28], in which the H_{29} cage surrounds Zr/Hf and a larger new H_{32} cage surrounds the Sr atoms. The $Cmmm$ $SrZrH_{14}$ has two new types of H_{28} and H_{30} cages, and these two H cages are not fully closed loop [see Fig. S3(c) of the SM [28]]. The predicted stable pressures of the above various clathrate structures are shown in Fig. 2(d), and the structural information is listed in Table S2 of the SM [28]. The searching results demonstrate that compensatory cosubstitution provides an effective route to designing new clathrate hydrides that possess superior superconductivity.

We next calculate their T_c's based on the anisotropic Migdal-Eliashberg formalism [74,75], estimated using the typical Coulomb pseudopotentials of $\mu^* = 0.1$ and 0.13 [15,17,76], as shown in Fig. 2(e). Among them, $CaHfH_{12}$ exhibits the highest T_c of 351–363 K at 300 GPa, much higher than those of CaH_6 (~230 K [12]) and HfH_6 (~55 K [72])

with the same stoichiometry ratio of H/metal. As the pressure decreases to 200 GPa, the T_c of $CaHfH_{12}$ still reaches ~350 K. Likewise, the T_c of $CaZrH_{12}$ is estimated to be as high as 343 K at 300 GPa, decreasing linearly to 296 K at 200 GPa. In addition, the T_c's of $CaZrH_{18}$, $CaHfH_{18}$, $SrZrH_{19}$, and $SrHfH_{19}$ with the hcp structure are predicted to be 329, 338, 263, and 305 K, respectively. We note that the theoretically predicted YH_{10} has the highest T_c of ~326 K among all the binary hydrides within comparable numerical accuracy, while these ternary hydrides $CaHfH_{12}$, $CaZrH_{12}$, $CaZrH_{18}$, and $CaHfH_{18}$ discovered here possess much higher T_c's, indicating that the multicomponent alloying approach with EMV = 3 can effectively enhance the superconductivity of the ternary hydrides.

To further reveal how such compensatory cosubstitution behaves synergistically to enhance superconductivity, we make comparative discussions of $CaHfH_{12}$ and YH_6 as well as $CaHfH_{18}$ and YH_9, which each pair has the same geometrical structure, respectively. The calculated electronic densities of states are displayed in Fig. 3(a), together with the electron-phonon coupling (EPC) and the atom-projected band structures in Figs. S4– S8 of the SM [28]. For YH_6 [Fig. 3(a)], the electronic occupation of the Y atomic orbitals is relatively higher than that of the antibonding σ^* orbitals of the H sublattice near the E_F. But for $CaHfH_{12}$ and $CaHfH_{18}$, the electronic occupations of the antibonding σ^* orbitals of the H sublattice become dominant in both cases. Quantitatively, our Bader charge analysis [77] shows that the Ca and Hf atoms transfer 0.92 and 1.71 e^- to a H_2 cage in $CaHfH_{12}$, respectively, with ~0.44 e^- accepted by each H_2 molecule, higher than 0.40 e^- per H_2 molecule in YH_6 [see Fig. 3(b)]. When comparing $CaHfH_{18}$ with YH_9, we reach the same conclusion [see Figs. 3(a) and 3(b)]. In short, the compensatory cosubstitution approach effectively increases the electronic occupation of the H sublattice, and then enhances the T_c.

Figure 3(c) is the integrated EPC constants $\lambda(\omega)$ for selective systems. Combined with other relevant quantities in Figs. S4– S6 of the SM [28], we see that the low-frequency phonon bands mainly originate from the vibrations of the metal atoms, while the high-frequency bands come from vibrations of the H sublattice. Furthermore, λ_{qv} reveals stronger contributions of the vibration modes of the H sublattice to the overall EPC. Specifically, the total λ of $CaHfH_{12}$ and $CaHfH_{18}$ are 2.09 and 2.11, with about 75%–80% is contributed by the H sublattice, respectively. In contrast, the total λ of YH_6 has a relatively smaller value of 1.76, and only about 55% by the H sublattice.

In addition, we note that there typically exist several bands crossing the Fermi surface (FS) of a given hydride (see Figs. S9 and S10 of the SM [28]). Accordingly, we evaluate the k-resolved EPC constant λ_{nk} to reflect the coupling strength of the phonons with each electron band and the anisotropic nature of the superconducting gap Δ_{nk} [74,75]. For simplicity, we present the results of $CaHfH_{12}$ in comparison with YH_6 [see Fig. 3(d)]. We see that the λ_{nk} values of $CaHfH_{12}$ and YH_6 scale with the weights of the H electronic states on the FS, and large EPC is observed for both systems due to the existing FS nesting, as shown in Fig. S11 of the SM [28]. It is noteworthy that the maximum value of λ_{nk} is 3.5 for $CaHfH_{12}$, which is much larger than that of ~2.7 for YH_6, implying that $CaHfH_{12}$ has stronger EPC on the FS. The largest values of the Δ_{nk} were estimated to be ~80 meV for $CaHfH_{12}$ and ~62 meV for YH_6. The corresponding T_c's were evaluated to be ~363 and 265 K for $CaHfH_{12}$ and YH_6, respectively (see Fig. S12 of the SM [28]). Clearly, these results provide strong evidence that the compensatory cosubstitution approach can not only promote the metallization of the H sublattice, but also enhance the EPC and hence, the T_c's.

In Fig. 4(a), we summarize the obtained T_c's of these hydrides as a function of the stoichiometric ratio of H/metal. For given a stoichiometric ratio, as long as the EMV of the substituted diatomic metals is 3, the T_c's of the ternary hydride are substantially higher than that of the binary hydride composed of a single metal element. Pronouncedly, the T_c is increased from ~120 K of LaH_8 to ~320 K of $SrZrH_{16}$, by nearly three times. Furthermore, the FMOs of the ternary hydrides are effectively adjusted with different ion radii, thereby providing the possibility of reducing their stabilizing pressures. We also note that although the crystal structures and the configurations of the H sublattices of these hydrides are quite different from system to system, they all obey the two aforementioned rules, showing that they hold true for binary, ternary, and potentially even higher multiple-component metal hydrides. Moreover, we also see that the empirical merit function S [78] of newly predicted ternary hydrides are comparable or superior to the binary hydrides, with $CaHfH_{12}$ having the largest S value of 1.78 [see Fig. 4(b)].

Aside from the T_c's, we finally examine the potential lower pressure aspect by calculating the FMOs of the ternary hydrides. The results are displayed in Figs. 4(c)– 4(f) for different stoichiometry ratios of H/metal. Strikingly, given a specific H/metal ratio, the binary and ternary hydrides follow the same linear scaling relationship between the minimal pressures to stabilize the structures and the FMOs. For example, the FMOs of $CaHfH_{12}/CaZrH_{12}$ are calculated to be ~0.34, located between ~0.32 of ZrH_6/HfH_6 and 0.37 of CaH_6. This means that the chemical pressure provided by the metal skeleton of CaZr/CaHf in $CaZrH_{12}/CaHfH_{12}$ is higher than that of Zr/Hf in ZrH_6/HfH_6, and smaller than that of Ca in CaH_6. The calculated minimum stabilizing pressures of $CaHfH_{12}/CaZrH_{12}$ are about 190 and 200 GPa, respectively, which qualitatively fit well the linear scaling relationship shown in Fig. 4(c).

In conclusion, we have conceptualized two empirical yet generic rules surrounding the T_c's and the minimum stabilizing pressures of metal hydride superconductors. By using the particle swarm optimization and first-principles calculations, we have not only predicted a collection of new hydride superconductors, including the representative examples of $CaHfH_{12}$, with T_c of ~360 K at 300 GPa, and $CaZrH_{12}$, with T_c of ~290 K at 200 GPa, but also shown that these rules hold true for binary, ternary, and even potentially higher multiple-component metal hydrides. Our findings will play an important role in predictive design of high-T_c hydride superconductors at lower pressures.

We acknowledge Jiantao Wang for valuable discussions and support from the National Natural Science Foundation of China (Grants No. 12104129, No. 12074099, No. 12174170,

and No. 11974323), Innovation Program for Quantum Science and Technology (Grant No. 2021ZD0302800), and Anhui Initiative in Quantum Information Technologies (Grant No. AHY170000).

[1] J. A. Flores-Livas, L. Boeri, A. Sanna, G. Profeta, R. Arita, and M. Eremets, Phys. Rep. **856**, 1 (2020).
[2] I. I. Mazin, Nature (London) **525**, 40 (2015).
[3] J. Bardeen, L. N. Cooper, and J. R. Schrieffer, Phys. Rev. **106**, 162 (1957).
[4] N. W. Ashcroft, Phys. Rev. Lett. **21**, 1748 (1968).
[5] J. M. McMahon and D. M. Ceperley, Phys. Rev. B **84**, 144515 (2011).
[6] J. M. McMahon, M. A. Morales, C. Pierleoni, and D. M. Ceperley, Rev. Mod. Phys. **84**, 1607 (2012).
[7] P. Dalladay-Simpson, R. T. Howie, and E. Gregoryanz, Nature (London) **529**, 63 (2016).
[8] P. Dias Ranga and F. Silvera Isaac, Science **355**, 715 (2017).
[9] P. Loubeyre, F. Occelli, and P. Dumas, Nature (London) **577**, 631 (2020).
[10] P. Cudazzo, G. Profeta, A. Sanna, A. Floris, A. Continenza, S. Massidda, and E. K. U. Gross, Phys. Rev. Lett. **100**, 257001 (2008).
[11] N. W. Ashcroft, Phys. Rev. Lett. **92**, 187002 (2004).
[12] H. Wang, J. S. Tse, K. Tanaka, T. Iitaka, and Y. Ma, Proc. Natl. Acad. Sci. USA **109**, 6463 (2012).
[13] Y. Li, J. Hao, H. Liu, J. S. Tse, Y. Wang, and Y. Ma, Sci. Rep. **5**, 9948 (2015).
[14] D. Duan, Y. Liu, F. Tian, D. Li, X. Huang, Z. Zhao, H. Yu, B. Liu, W. Tian, and T. Cui, Sci. Rep. **4**, 6968 (2014).
[15] F. Peng, Y. Sun, C. J. Pickard, R. J. Needs, Q. Wu, and Y. Ma, Phys. Rev. Lett. **119**, 107001 (2017).
[16] Z. Zhang, T. Cui, M. J. Hutcheon, A. M. Shipley, H. Song, M. Du, V. Z. Kresin, D. Duan, C. J. Pickard, and Y. Yao, Phys. Rev. Lett. **128**, 047001 (2022).
[17] H. Liu, I. I. Naumov, R. Hoffmann, N. W. Ashcroft, and R. J. Hemley, Proc. Natl. Acad. Sci. USA **114**, 6990 (2017).
[18] D. V. Semenok, I. A. Kruglov, I. A. Savkin, A. G. Kvashnin, and A. R. Oganov, Curr. Opin. Solid State Mater. Sci. **24**, 100808 (2020).
[19] G. Gao, L. Wang, M. Li, J. Zhang, R. T. Howie, E. Gregoryanz, V. V. Struzhkin, L. Wang, and J. S. Tse, Mater. Today Phys. **21**, 100546 (2021).
[20] E. Zurek and T. Bi, J. Chem. Phys. **150**, 050901 (2019).
[21] E. Snider, N. Dasenbrock-Gammon, R. McBride, M. Debessai, H. Vindana, K. Vencatasamy, K. V. Lawler, A. Salamat, and R. P. Dias, Nature (London) **586**, 373 (2020).
[22] A. P. Drozdov, M. I. Eremets, I. A. Troyan, V. Ksenofontov, and S. I. Shylin, Nature (London) **525**, 73 (2015).
[23] A. P. Drozdov, P. P. Kong, V. S. Minkov, S. P. Besedin, M. A. Kuzovnikov, S. Mozaffari, L. Balicas, F. F. Balakirev, D. E. Graf, V. B. Prakapenka, E. Greenberg, D. A. Knyazev, M. Tkacz, and M. I. Eremets, Nature (London) **569**, 528 (2019).
[24] M. Somayazulu, M. Ahart, A. K. Mishra, Z. M. Geballe, M. Baldini, Y. Meng, V. V. Struzhkin, and R. J. Hemley, Phys. Rev. Lett. **122**, 027001 (2019).
[25] P. Kong, V. S. Minkov, M. A. Kuzovnikov, A. P. Drozdov, S. P. Besedin, S. Mozaffari, L. Balicas, F. F. Balakirev, V. B. Prakapenka, S. Chariton *et al.*, Nat. Commun. **12**, 5075 (2021).
[26] Z. Li, X. He, C. Zhang, X. Wang, S. Zhang, Y. Jia, S. Feng, K. Lu, J. Zhao, J. Zhang *et al.*, Nat. Commun. **13**, 2863 (2022).
[27] L. Ma, K. Wang, Y. Xie, X. Yang, Y. Wang, M. Zhou, H. Liu, X. Yu, Y. Zhao, H. Wang *et al.*, Phys. Rev. Lett. **128**, 167001 (2022).
[28] See Supplemental Material at http://link.aps.org/supplemental/10.1103/PhysRevB.107.L020504 for the computational method, calculated fractional metal occupancy of hydride superconductors, configurations of predicted ternary hydrides, the linear scaling relationship, convex hull of ternary hydrides, phonon spectra, the total EPC constant, electronic density of states, band structures, Fermi surface, and superconducting gaps of $CaHfH_{12}$ and YH_6, which includes Refs. [29–66].
[29] J. Lv, Y. Wang, L. Zhu, and Y. Ma, Phys. Rev. Lett. **106**, 015503 (2011).
[30] L. Zhu, H. Wang, Y. Wang, J. Lv, Y. Ma, Q. Cui, Y. Ma, and G. Zou, Phys. Rev. Lett. **106**, 145501 (2011).
[31] B. Gao, P. Gao, S. Lu, J. Lv, Y. Wang, and Y. Ma, Sci. Bull. **64**, 301 (2019).
[32] H. Wang, Y. Wang, J. Lv, Q. Li, L. Zhang, and Y. Ma, Comput. Mater. Sci. **112**, 406 (2016).
[33] G. Kresse and J. Furthmüller, Phys. Rev. B **54**, 11169 (1996).
[34] P. E. Blöchl, Phys. Rev. B **50**, 17953 (1994).
[35] G. Kresse and D. Joubert, Phys. Rev. B **59**, 1758 (1999).
[36] J. P. Perdew, K. Burke, and M. Ernzerhof, Phys. Rev. Lett. **77**, 3865 (1996).
[37] P. Giannozzi, S. Baroni, N. Bonini, M. Calandra, R. Car, C. Cavazzoni, D. Ceresoli, G. L. Chiarotti, M. Cococcioni, I. Dabo *et al.*, J. Phys.: Condens. Matter **21**, 395502 (2009).
[38] M. J. van Setten, M. Giantomassi, E. Bousquet, M. J. Verstraete, D. R. Hamann, X. Gonze, and G. M. Rignanese, Comput. Phys. Commun. **226**, 39 (2018).
[39] F. Giustino, M. L. Cohen, and S. G. Louie, Phys. Rev. B **76**, 165108 (2007).
[40] S. Poncé, E. R. Margine, C. Verdi, and F. Giustino, Comput. Phys. Commun. **209**, 116 (2016).
[41] Y. Xie, Q. Li, A. R. Oganov, and H. Wang, Acta Crystallogr. Sect. C: Struct. Chem. **70**, 104 (2014).
[42] P. Hou, X. Zhao, F. Tian, D. Li, D. Duan, Z. Zhao, B. Chu, B. Liu, and T. Cui, RSC Adv. **5**, 5096 (2015).
[43] D. V. Semenok, A. G. Kvashnin, I. A. Kruglov, and A. R. Oganov, J. Phys. Chem. Lett. **9**, 1920 (2018).
[44] W. Sun, X. Kuang, H. D. J. Keen, C. Lu, and A. Hermann, Phys. Rev. B **102**, 144524 (2020).
[45] H. Song, Z. Zhang, T. Cui, C. J. Pickard, V. Z. Kresin, and D. Duan, Chin. Phys. Lett. **38**, 107401 (2021).
[46] J. Zhao, B. Ao, S. Li, T. Gao, and X. Ye, J. Phys. Chem. C **124**, 7361 (2020).
[47] Y.-L. Hai, N. Lu, H.-L. Tian, M.-J. Jiang, W. Yang, W.-J. Li, X.-W. Yan, C. Zhang, X.-J. Chen, and G.-H. Zhong, J. Phys. Chem. C **125**, 3640 (2021).
[48] I. A. Kruglov, G. K. Alexander, F. G. Alexander, R. O. Artem, S. Lobanov Sergey, N. Holtgrewe, S. Jiang, B. P. Vitali,

E. Greenberg, and V. Yanilkin Alexey, Sci. Adv. **4**, eaat9776 (2020).
[49] Y. Liu, D. Duan, F. Tian, H. Liu, C. Wang, X. Huang, D. Li, Y. Ma, B. Liu, and T. Cui, Inorg. Chem. **54**, 9924 (2015).
[50] X. Li and F. Peng, Inorg. Chem. **56**, 13759 (2017).
[51] A. G. Kvashnin, D. V. Semenok, I. A. Kruglov, I. A. Wrona, and A. R. Oganov, ACS Appl. Mater. Interfaces **10**, 43809 (2018).
[52] D. V. Semenok, A. G. Kvashnin, A. G. Ivanova, V. Svitlyk, V. Y. Fominski, A. V. Sadakov, O. A. Sobolevskiy, V. M. Pudalov, I. A. Troyan, and A. R. Oganov, Mater. Today **33**, 36 (2020).
[53] X. Li, H. Liu, and F. Peng, Phys. Chem. Chem. Phys. **18**, 28791 (2016).
[54] R. Szczęániak and A. P. Durajski, Supercond. Sci. Technol. **27**, 015003 (2014).
[55] D. Y. Kim, R. H. Scheicher, C. J. Pickard, R. J. Needs, and R. Ahuja, Phys. Rev. Lett. **107**, 117002 (2011).
[56] S. Yu, X. Jia, G. Frapper, D. Li, A. R. Oganov, Q. Zeng, and L. Zhang, Sci. Rep. **5**, 17764 (2015).
[57] K. Abe, Phys. Rev. B **96**, 144108 (2017).
[58] D. Zhou, V. S. Dmitrii, D. Duan, H. Xie, W. Chen, X. Huang, X. Li, B. Liu, R. O. Artem, and T. Cui, Sci. Adv. **6**, eaax6849 (2020).
[59] X. Feng, J. Zhang, G. Gao, H. Liu, and H. Wang, RSC Adv. **5**, 59292 (2015).
[60] X. Liang, A. Bergara, L. Wang, B. Wen, Z. Zhao, X.-F. Zhou, J. He, G. Gao, and Y. Tian, Phys. Rev. B **99**, 100505 (2019).
[61] P. Song, Z. Hou, P. B. de Castro, K. Nakano, Y. Takano, R. Maezono, and K. Hongo, Adv. Theory Simul. **5**, 2100364 (2022).
[62] P. Song, Z. Hou, P. B. D. Castro, K. Nakano, K. Hongo, Y. Takano, and R. Maezono, Chem. Mater. **33**, 9501 (2021).
[63] L.-T. Shi, Y.-K. Wei, A. K. Liang, R. Turnbull, C. Cheng, X.-R. Chen, and G.-F. Ji, J. Mater. Chem. C **9**, 7284 (2021).
[64] W. Sukmas, P. Tsuppayakorn-aek, U. Pinsook, and T. Bovornratanaraks, J. Alloys. Compd. **849**, 156434 (2020).
[65] J. Bi, Y. Nakamoto, P. Zhang, K. Shimizu, B. Zou, H. Liu, M. Zhou, G. Liu, H. Wang, and Y. Ma, Nat. Commun. **13**, 5952 (2022).
[66] Q. Wu, S. Zhang, H.-F. Song, M. Troyer, and A. A. Soluyanov, Comput. Phys. Commun. **224**, 405 (2018).
[67] C. Heil, S. di Cataldo, G. B. Bachelet, and L. Boeri, Phys. Rev. B **99**, 220502(R) (2019).
[68] Y. Wang, J. Lv, L. Zhu, and Y. Ma, Comput. Phys. Commun. **183**, 2063 (2012).
[69] Y. Wang, J. Lv, L. Zhu, and Y. Ma, Phys. Rev. B **82**, 094116 (2010).
[70] Y. Wang, H. Wang, J. S. Tse, T. Iitaka, and Y. Ma, Phys. Chem. Chem. Phys. **17**, 19379 (2015).
[71] K. Abe, Phys. Rev. B **98**, 134103 (2018).
[72] H. Xie, Y. Yao, X. Feng, D. Duan, H. Song, Z. Zhang, S. Jiang, S. A. T. Redfern, V. Z. Kresin, C. J. Pickard, and T. Cui, Phys. Rev. Lett. **125**, 217001 (2020).
[73] L. Liu, C. Wang, S. Yi, K. W. Kim, J. Kim, and J.-H. Cho, Phys. Rev. B **99**, 140501(R) (2019).
[74] H. J. Choi, M. L. Cohen, and S. G. Louie, Phys. C: Superconductivity **385**, 66 (2003).
[75] A. Sanna, J. A. Flores-Livas, A. Davydov, G. Profeta, K. Dewhurst, S. Sharma, and E. K. U. Gross, J. Phys. Soc. Jpn. **87**, 041012 (2018).
[76] C. Wang, S. Yi, and J.-H. Cho, Phys. Rev. B **101**, 104506 (2020).
[77] E. Sanville, S. D. Kenny, R. Smith, and G. Henkelman, J. Comput. Chem. **28**, 899 (2007).
[78] C. J. Pickard, I. Errea, and M. I. Eremets, Annu. Rev. Condens. Matter Phys. **11**, 57 (2020).